InGaN-Based p–i–n Solar Cells with Graphene Electrodes

Jae-Phil Shim, Minhyeok Choe[1], Seong-Ran Jeon[2], Dongju Seo, Takhee Lee[1], and Dong-Seon Lee

School of Information and Communications, Gwangju Institute of Science and Technology, Gwangju 500-712, Korea
[1]School of Materials Science and Engineering, Gwangju Institute of Science and Technology, Gwangju 500-712, Korea
[2]Korea Photonics Technology Institute, Gwangju 500-712, Korea

InGaN-based p–i–n solar cells with graphene electrodes were fabricated and compared with solar cells using indium tin oxide (ITO) electrodes. In particular, we analyzed the properties of graphene film by means of high-resolution transmission electron microscopic (HRTEM) and Raman spectroscopy, also comparing optical properties with those of ITO, conventionally used as transparent electrodes. The solar cells using graphene revealed a short circuit current density of 0.83 mA/cm^2, an open circuit voltage of 2.0 V, a fill factor of 75.2%, and conversion efficiency of 1.2%, comparable to the performance of solar cells using ITO. © 2011 The Japan Society of Applied Physics

InGaN materials have been examined extensively for solar cell application due to their tunable band gap energy range of 0.7 to 3.4 eV, which is applicable to the entire functional range of the solar spectrum.[1,2] As for p-type metal contacts, Ni/Au semitransparent layers, with excellent Ohmic properties, have been predominantly used in InGaN-based solar cells for current spreading.[3,4] However, by balancing the transparency and ohmic properties of transparent electrodes, enhancing electron extraction from InGaN absorption regions to metal electrodes under light illumination has become viable. In our previous work, we demonstrated that indium tin oxide (ITO) works better than Ni/Au for current spreading layers in InGaN-based solar cells mostly due to its better transmittance, and also demonstrated improved conversion efficiency.[5] Although advanced solar cell performance has been obtained using ITO transparent electrodes, ITO also has limitations such as increasing cost due to indium scarcity, limited transparency at near UV and IR regions, and a sensitivity to acidic and base chemical sources. Furthermore, ITO can easily crack and break when deposited on bending substrates, making it difficult to use for applications such as flexible displays and touch screens. Therefore, a new transparent contact material is needed for efficiency and improved performance. As an alternative, graphene has attracted vast interest for optoelectronic applications, such as transparent electrodes in solar cells and light emitting diodes, due to its outstanding optical and electrical properties, i.e., high mobility, transparency, flexibility, and mechanical and chemical stability.[6–9] In particular, graphene film grown by chemical vapor deposition (CVD) is more advantageous than film prepared by other methods, such as the scotch tape method, due to the simple transferability to arbitrary substrates with large-scale and uniform conductivity.[10,11] We applied a graphene film produced by CVD methods as a transparent contact layer in InGaN-based solar cells. In this study, we investigated the photovoltaic performance of an InGaN solar cell by comparing the optical properties of graphene and ITO utilized as contact layers.

InGaN/GaN p–i–n structures were grown using metal organic CVD (MOCVD). The epitaxial structures consisted of an undoped GaN/Al$_2$O$_3$ template, a 2.2-μm Si-doped n-GaN layer, a 200-nm intrinsic InGaN layer, and a 100-nm Mg doped p-GaN layer. An intrinsic InGaN layer was grown at 805 °C, and the In composition of the InGaN layer was determined by X-ray diffraction (XRD) at 10.8%, as shown Fig. 1(a). We fabricated two sets of 1 × 1 mm^2 solar cells on an epitaxial structure with ITO and graphene current

(a)

(b)
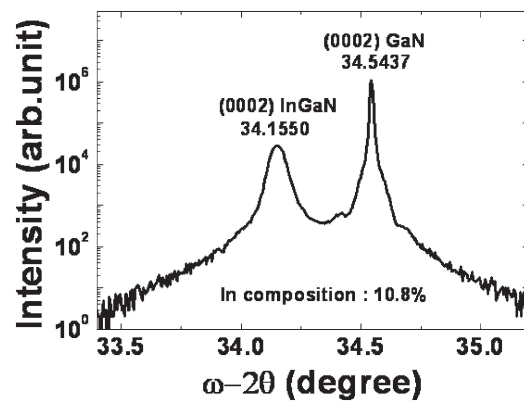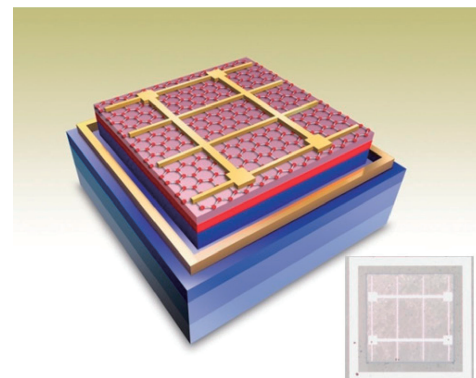
Fig. 1. (a) ω–2θ XRD scan curve of (0002) InGaN and GaN peaks. (b) Schematic of fabricated device with a graphene current spreading layer. Inset is a top view of a real optical image of a fabricated device.

spreading layers. The fabrication of solar cells with ITO have been utilized a previously reported process.[5] When ITO was used as a current spreading layer, we annealed the device at 500 °C for 1 min under ambient condition to enhance Ohmic characteristics.[12,13] For the graphene-based device, graphene was grown separately on a 300 nm thick Ni-deposited substrate at 1,000 °C under a CH$_4$ gas flow and 4% H$_2$ in an Ar gas mixture for 5 min by means of CVD. Subsequently, the graphene-grown substrate was abruptly cooled to room temperature (>200 °C/min) to suppress excessive carbon atom precipitation. After film growth, graphene was released from the substrate by etching Ni in an aqueous iron chloride (FeCl$_3$) solution. The released graphene film was transferred physically onto the top surface

© 2011 The Japan Society of Applied Physics

(a)

(b)
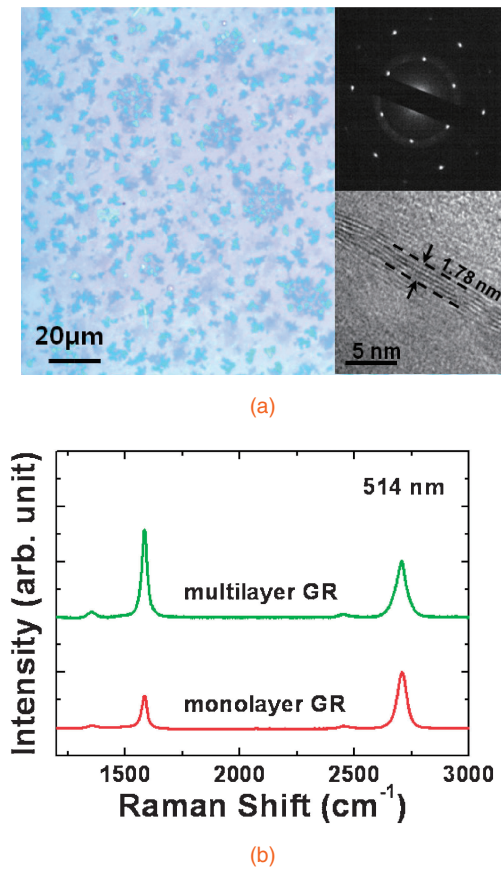
Fig. 2. (a) Optical image of graphene film. Upper inset is an electron diffraction image. Lower inset is a cross-sectional HRTEM image. (b) Raman spectra of graphene films.

(a)

(b)
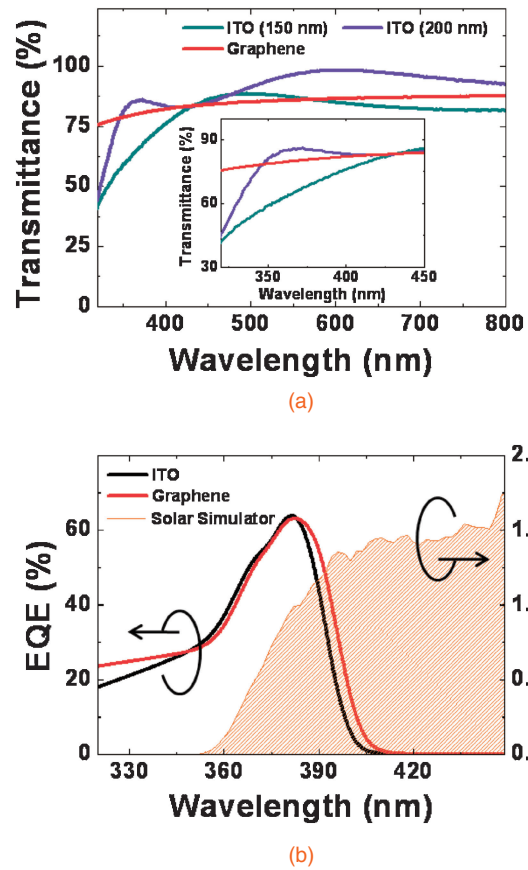
Fig. 3. (a) Transmittance of ITO and graphene films. (b) External quantum efficiency of fabricated devices with ITO and graphene current spreading layers. Shaded area denotes solar spectrum.

of the prepared epitaxial structure as a current spreading layer. Graphene, having 4.5 eV work function, revealed slightly lower Schottky barrier with p-GaN than ITO which shows 4.3 eV work function.[14,15] Covered with a patterned protective photoresist (PR) etch mask, graphene and GaN layers were etched sequentially using inductively coupled plasma (ICP) until n-GaN was revealed. Afterward, a Ni/Au (30 nm/500 nm) p-contact pad was formed on graphene, and a Ti/Al/Ti/Au (30 nm/50 nm/30 nm/500 nm) n-contact was deposited on the exposed n-GaN by an e-beam evaporator. Figure 1(b) shows a schematic of the fabricated device, and the inset represents the top image of the fabricated device.

The properties of the graphene film were investigated by optical microscopy and high-resolution transmission electron microscopy (HRTEM), being further confirmed by Raman spectroscopy. Figure 2(a) shows an optical image of the graphene film grown on a 300-nm-thick SiO_2 layer on the Si substrate. Our CVD-grown graphene films consisted of mono- to multi-layer regions; that is, the bright region possessed a thinner graphene film than the dark region. The electron diffraction (ED) image [upper inset of Fig. 2(a)] taken from the monolayer region reveals a hexagonal pattern, confirming the arrangement of carbon atoms in the graphene film. Furthermore, the cross-sectional HRTEM image [lower inset of Fig. 2(a)] of the multilayer graphene shows the number of graphene layers ($\sim$5) and the interlayer distance (3.5 ± 0.1 Å). In addition, Raman spectroscopy, which has become the standard analysis tool in the field of graphene research,

captured typical graphene spectra, as shown in Fig. 2(b). The integrated intensity ratio from the G peak ($\sim$1350 cm^{-1}) to the 2D peak ($\sim$2700 cm^{-1}) was related to the thickness of graphene films; that is, the high value of I_G/I_{2D} was in the multilayer region of the graphene film.

ITO films were deposited on glass under various thickness conditions, and their transmittances were compared with those of the graphene film. As shown in Fig. 3(a), ITO transmittances largely depended on thickness due to the interference effect of refracted lights at the top and bottom of the ITO film. Moreover, each ITO sample showed transmittance fluctuation, the largest gap being approximately 50%, within the measured wavelength range. While ITO transmittance changed due to wavelength, graphene, being very thin (below 10 nm), showed a constant transmittance of $\sim$80%. Although more transparent graphene with $\sim$90% transmittance could be grown at 800 °C, we used graphene grown at 1,000 °C, displaying 80% transmittance due to better electrical properties which is a critical factor for carrier extraction in solar cells. Based on our previous work, graphene grown at 800 and 1,000 °C displayed, respectively a sheet resistances of 1730 ± 600 and $610 \pm 140 \, \Omega/\square$ and mobilities of 660 ± 270 and $1180 \pm 260 \, cm^2 \, V^{-1} \, s^{-1}$.[14] Figure 3(b) displays the external quantum efficiency (EQE) of the fabricated devices. From ITO and the graphene sample, 65 and 63.6% peak EQEs were obtained, respectively. Both devices displayed a similar EQE shape, i.e., major light absorption occurred within a range of 360 to 410 nm. In spite of the higher transparency of graphene, as

© 2011 The Japan Society of Applied Physics
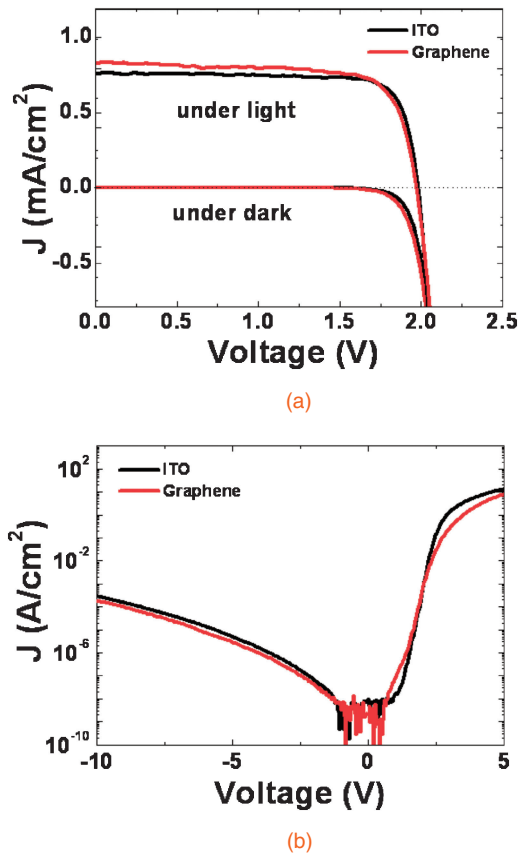
Fig. 4. (a) J–V characteristics measured under dark and light illumination. (b) Log-scaled dark current density.

Table I. Solar cell parameters for fabricated devices.

	V_{oc} (V)	J_{sc} (mA/cm^2)	FF (%)	Efficiency (%)
Graphene	2.0	0.83	75.2	1.2
ITO	2.0	0.76	79.7	1.2

it showed a larger leakage current under the forward bias, ranging from $\sim$0.5 to $\sim$2 V. Consequently, the larger leakage under the forward bias region increased the series resistance and reduced the device fill factor. The measured solar cell parameters were represented in Table I. The solar cell with graphene demonstrated 1.2% conversion efficiency, which was comparable with the results from the ITO sample. Although the graphene sample showed a lower FF than ITO, the slightly high J_{sc} supplemented the conversion efficiency.

In conclusion, we applied graphene as the current spreading layer in InGaN-based solar cells, and compared the results with those of ITO. While ITO revealed transmittance variation with thickness and wavelength, the thin-layered graphene maintained almost the same transmittance. The overall performance of the solar cell with graphene was comparable to that with ITO, and we verified the possibility of using graphene as a current spreading layer in InGaN-based solar cells. Further efficiency enhancement is expected in InGaN based solar cell using graphene since more graphene research is currently going along to enhance electrical properties such as control of graphene work function and improvement of mobility. Clearly, more effort should be exerted towards the optimization of graphene as a transparent contact material in facilitating discernible advantages such as high transparency, and flexibility, as well as mechanical and chemical stability.

opposed to the ITO below the $\sim$390-nm region, the EQE turned out to be very similar to that of the ITO sample. Such a result was likely due to less efficient electron extraction of graphene, coming from higher sheet resistance (610 $\pm$ 140 Ω/$\square$), than that of ITO (180 Ω/$\square$). The upper limit of the EQE spectrum was $\sim$410 nm for the graphene sample, while it was slightly longer than $\sim$405 nm for the ITO sample. A slight variation within the indium composition over the epilayer caused an eventual $\sim$5-nm increase in the upper EQE limit, resulting in a slightly higher EQE, ranging from 385 to 410 nm, in the graphene sample.

Figure 4(a) shows the current density relative to voltage (J–V) characteristics measured under darkened conditions and AM 1.5G light illumination. For both samples, 2 V of open circuit voltage (V_{oc}) was obtained. However, each sample revealed different short circuit current densities (J_{sc}) and fill factors (FF). The J_{sc} and the FF of the graphene sample were 0.831 mA/cm^2 and 75.2%, respectively, whereas for the ITO sample were 0.764 mA/cm^2 and 79.7%, respectively. The approximately 10% increase in the J_{sc} of the graphene sample could be explained by the overlapping EQE region of the graphene sample with the solar spectrum, which had a larger area than that of the ITO sample. In order to clarify the difference of the FF, we investigated the leakage by measuring the dark current density, plotted in Fig. 4(b) in log scale. Both samples showed a very low leakage current density, 10^{-9}–10^{-8} A/cm near 0 V. Although the solar cell with graphene revealed a slightly lower leakage current under reverse bias,

1) O. Jani, I. Ferguson, C. Honsberg, and S. Kurtz: Appl. Phys. Lett. **91** (2007) 132117.
2) C. J. Neufeld, N. G. Toledo, S. C. Cruz, M. Iza, S. P. DenBaars, and U. K. Mishra: Appl. Phys. Lett. **93** (2008) 143502.
3) R.-H. Horng, S.-T. Lin, Y.-L. Tsai, M.-T. Chu, W.-Y. Liao, M.-H. Wu, R.-M. Lin, and T.-C. Lu: IEEE Electron Device Lett. **30** (2009) 724.
4) R. Dahal, B. Pantha, J. Li, J. Y. Lin, and H. X. Jiang: Appl. Phys. Lett. **94** (2009) 063505.
5) J.-P. Shim, S.-R. Jeon, Y.-K. Jeong, and D.-S. Lee: IEEE Electron Device Lett. **31** (2010) 1140.
6) K. S. Novoselov, A. K. Geim, S. V. Morozov, D. Jiang, M. I. Katsnelson, I. V. Grigorieva, S. V. Dubonos, and A. A. Firsov: Nature **438** (2005) 197.
7) A. K. Geim and K. S. Novoselov: Nat. Mater. **6** (2007) 183.
8) C. Lee, X. Wei, J. W. Kysar, and J. Hone: Science **321** (2008) 385.
9) V. C. Tung, L.-M. Chen, M. J. Allen, J. K. Wassei, K. Nelson, R. B. Kaner, and Y. Yang: Nano Lett. **9** (2009) 1949.
10) A. Reina, X. Jia, J. Ho, D. Nezich, H. Son, V. Bulovic, M. S. Dresselhaus, and J. Kong: Nano Lett. **9** (2009) 30.
11) K. S. Kim, Y. Zhao, H. Jang, S. Y. Lee, J. M. Kim, K. S. Kim, J.-H. Ahn, P. Kim, J.-Y. Choi, and B. H. Hong: Nature **457** (2009) 706.
12) T. Margalith, O. Buchinsky, D. A. Cohen, A. C. Abare, M. Hansen, S. P. DenBaars, and L. A. Coldren: Appl. Phys. Lett. **74** (1999) 3930.
13) K.-M. Chang, J.-Y. Chu, and C.-C. Cheng: Solid-State Electron. **49** (2005) 1381.
14) M. Cheo, B. H. Lee, G. Jo, J. Park, W. Park, S. Lee, W.-K. Hong, M.-J. Seong, Y. H. Kahng, K. Lee, and T. Lee: Org. Electron. **11** (2010) 1864.
15) Y. J. Lin and C. W. Hsu: J. Electron. Mater. **33** (2004) 1036.

© 2011 The Japan Society of Applied Physics